Chemical Science

ROYAL SOCIETY OF CHEMISTRY

EDGE ARTICLE

View Article Online
View Journal

Cite this: DOI: 10.1039/d5sc09742h

All publication charges for this article have been paid for by the Royal Society of Chemistry

Received 11th December 2025
Accepted 20th March 2026

DOI: 10.1039/d5sc09742h

rsc.li/chemical-science

From alkynes to spiroindole δ-lactams *via* a copper-nitrenoid intermediate featuring unusual 1,1-addition and high *Z*-selectivity

Zhiqiang Ren, †* Tianhui Feng,† Yeyao Li, Mengyi Chu, Ye Zheng, Tianli Gao, Bo Han, Ruili Guo, Haojie Ma, Ji-Jiang Wang and Yuqi Zhang *

This study reports a novel, operationally efficient N-heterocyclic carbene (NHC)-copper-catalysed strategy for the synthesis of spiroindole δ-lactams *via* the coupling of dioxazolones with alkyne derivatives. The protocol demonstrates high atom economy, excellent product yields, broad functional group tolerance, and outstanding *Z*-stereoselectivity. Detailed mechanistic investigations, combining density functional theory (DFT) calculations with Kinetic isotope effect (KIE) experiments, reveal that the efficient formation of the copper alkyne intermediate is the key factor governing the progression of this transformation. The observed 1,1-addition of unactivated alkynes, delivering high *Z*/*E* stereoselectivity and excellent regioselectivity, is proposed to proceed *via* a hydrogen atom migration mechanism.

Introduction

Lactam scaffolds are ubiquitous in agrochemicals, pharmaceuticals, and natural products, serving as privileged structural motifs that confer diverse biological activities and substantial clinical significance.[1–3] The alkaloid (−)-spiroquinazoline, distinguished by its unique spiroindole δ-lactam architecture,[4–6] together with related congeners, has been reported to display significant anticancer activity[7,8] (Scheme 1(1)). Accordingly, establishing operationally simple, efficient, and scalable methodologies for lactam synthesis is a significant objective in contemporary synthetic chemistry, with substantial academic and industrial implications.

Metallonitrenes are highly versatile reactive intermediates that have been widely exploited for the efficient assembly of polycyclic lactam frameworks through transition metal-catalyzed (Rh, Ir, Ni, Fe) direct C–N bond-forming reactions with alkynes.[9–22] For example, Blakey *et al.* reported a rhodium-catalyzed strategy for the synthesis of polycyclic lactam frameworks from sulfonamides and alkynes (Scheme 1(2)a);[23–26] Similarly, Chang *et al.* demonstrated that Ir- and Ni-catalyzed reactions of dioxazolones with alkynes proceed with high regioselectivity encompassing both 5-*exo* and 6-*endo* cyclization pathways and excellent stereoselectivity, affording defined *Z*/*E* configuration (Scheme 1(2)b).[27–29] In addition, significant advances have been achieved in the direct formation of N–N, N–C, and N–S bonds through transition metal-catalysed (*e.g.*, Ir, Rh, Fe, Cu, Mn) transformations of dioxazolones *via* metallonitrene intermediates.[30–41] However, the copper-catalyzed

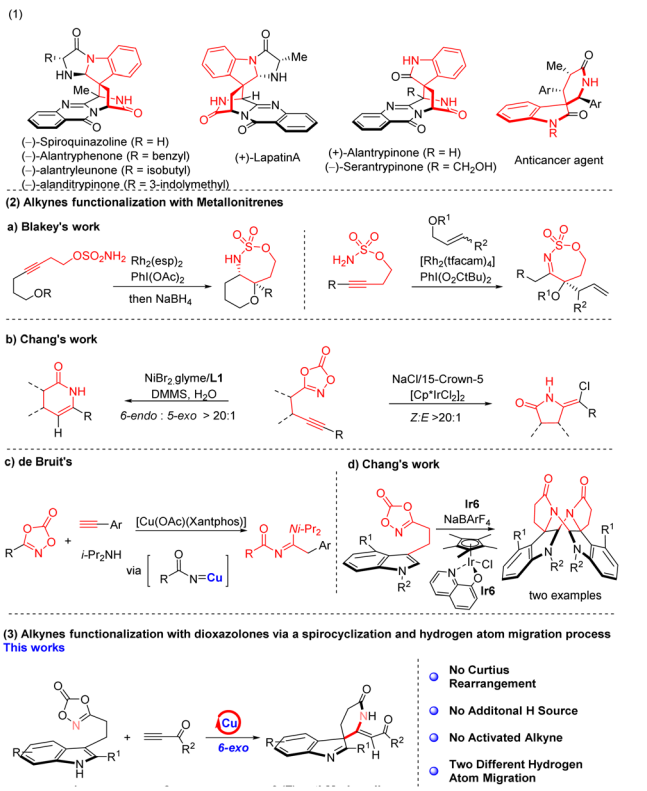

Scheme 1 Chemo-, regio-, and stereoselectivity functionalization of alkynes.

Department of New Energy & New Functional Materials, Shaanxi Key Laboratory of Chemical Reaction Engineering, School of Chemistry and Chemical Engineerin Yan'an University, Yan'an, 716000, P. R. China. E-mail: renzhiqiang@yau.edu.cn; yqzhang@yau.edu.cn

† F Z.R. and T.F. contributed equally to this work.

construction of polycyclic lactams from alkynes and dioxazolones *via* metallonitrene intermediates remains unexplored. To date, only de Bruin *et al.* have reported a related copper-mediated three-component transformation involving dioxazolones, alkynes, and diisopropylamine, leading to the formation of distinctive amidine scaffolds (Scheme 1(2)c).[42]

Indole derivatives are well recognized for their diverse biological activities and significant medicinal relevance,[43–45] and extensive efforts have been devoted to their dearomatization.[46–49] In this context, Chang *et al.* reported an iridium (Ir)-catalyzed transformation of indoles with dioxazolones, leading to the formation of an unusual dimeric framework (Scheme 1(2)c).[50] The synthesis of indole-containing polycyclic lactam architectures has garnered significant interest in recent years. In the present study, alkynes were strategically incorporated into the reaction system to enable the construction of a spiroindole δ-lactam framework. Notably, the reaction proceeds without undergoing a Curtius rearrangement and instead furnishes the anti-Markovnikov 1,1-addition product *via* a 6-*exo* cyclization pathway, delivering compound **3** with high *Z*-selectivity (Scheme 1(3)).

Results and discussion

Dioxazolone **1a** and methyl propiolate **2a** were selected as model substrates for reaction optimization (Table 1). Under the initial conditions using IPrCuCl as the catalyst, AgOAc as the additive, and 1,2-dichloroethane (DCE) as the solvent at 80 °C for 15 min, the desired product **3a** was obtained in 77% isolated yield (Table 1, entry 1). The molecular structure of compound **3a** was unambiguously established by single-crystal X-ray diffraction (XRD), nuclear magnetic resonance (NMR) spectroscopy, and high-resolution mass spectrometry (HRMS). The *Z* configuration was primarily determined based on NMR analysis and corroborated by XRD data. Subsequently, the influence of different copper catalysts, including $Cu(OAc)_2$, CuCl, and IMesCuCl, on the reaction outcome was systematically evaluated (Table 1, entries 2–4). It was observed that although the *Z*/*E* ratio remained essentially unchanged, the product yield decreased to 20–38%. To further evaluate the influence of additives, various silver salts, including $AgNO_3$, AgOTf, $AgSbF_6$, and $AgNTf_2$, were systematically examined. In all cases, the *Z*/*E* ratio was maintained; however, the yields were significantly reduced to 13–26% (Table 1, entries 5–8). To enhance the reaction efficiency, the catalyst loading was increased to 15 mol%, and the additive loading to 30 mol%. Under these optimized conditions, the isolated yield was 88%, while maintaining excellent stereoselectivity (*Z*/*E* > 20 : 1; Table 1, entry 9). Furthermore, the choice of solvent significantly influenced the reaction outcome. When DCM or $CHCl_3$ was employed as the solvent, the isolated yield decreased to 67–68% (Table 1, entries 10–11). The reaction temperature was also found to influence the transformation significantly. Lowering the temperature to 60 °C decreased the yield and prolonged the reaction time to 1 h (Table 1, entry 12).

To further optimize and validate the established reaction conditions, a systematic evaluation of substrate scope and functional group tolerance was conducted (Scheme 2). Various

Table 1 Optimization of reaction conditions for the synthesis of spiroindole δ-lactam using dioxazolone and methyl propiolate[a]

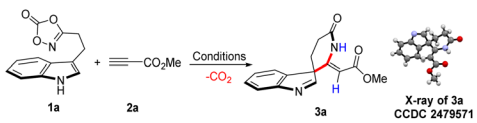

Entry	Catalyst	Additive	Solvent	*T*/°C	Yield%[b]	*Z*/*E*[c]
1	IPrCuCl(10 mol%)	AgOAc(20 mol%)	DCE	80	77	>20 : 1
2	$Cu(OAc)_2$(10 mol%)	AgOAc(20 mol%)	DCE	80	38	>20 : 1
3	CuCl(10 mol%)	AgOAc(20 mol%)	DCE	80	28	>20 : 1
4	IMesCuCl(10 mol%)	AgOAc(20 mol%)	DCE	80	20	>20 : 1
5	IPrCuCl(10 mol%)	AgOAc(20 mol%)	DCE	80	18	>20 : 1
6	IPrCuCl(10 mol%)	AgOAc(20 mol%)	DCE	80	15	>20 : 1
7	IPrCuCl(10 mol%)	AgOAc(20 mol%)	DCE	80	26	>20 : 1
8	IPrCuCl(10 mol%)	AgOAc(20 mol%)	DCE	80	13	>20 : 1
9	**IPrCuCl(10 mol%)**	**AgOAc(20 mol%)**	**DCE**	**80**	**88**	**>20 : 1**
10	IPrCuCl(10 mol%)	AgOAc(20 mol%)	CH_2Cl_2	80	69	>20 : 1
11	IPrCuCl(10 mol%)	AgOAc(20 mol%)	$CHCl_3$	80	67	>20 : 1
12[d]	IPrCuCl(10 mol%)	AgOAc(20 mol%)	DCE	80	68	>20 : 1

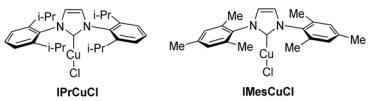

[a] Reaction conditions: **1a** (0.20 mmol), **2a** (0.60 mmol), Cu catalyst (× mol%), Ag salt (2× mol%), 80 °C, 15 min, 0.05 M, under air. [b] Isolated yields. [c] *Z*/*E* ratio determined by NMR and XRD. [d] Reaction time: 1 h. Abbreviations: DCE = 1,2-dichloroethane; DCM = dichloromethane.

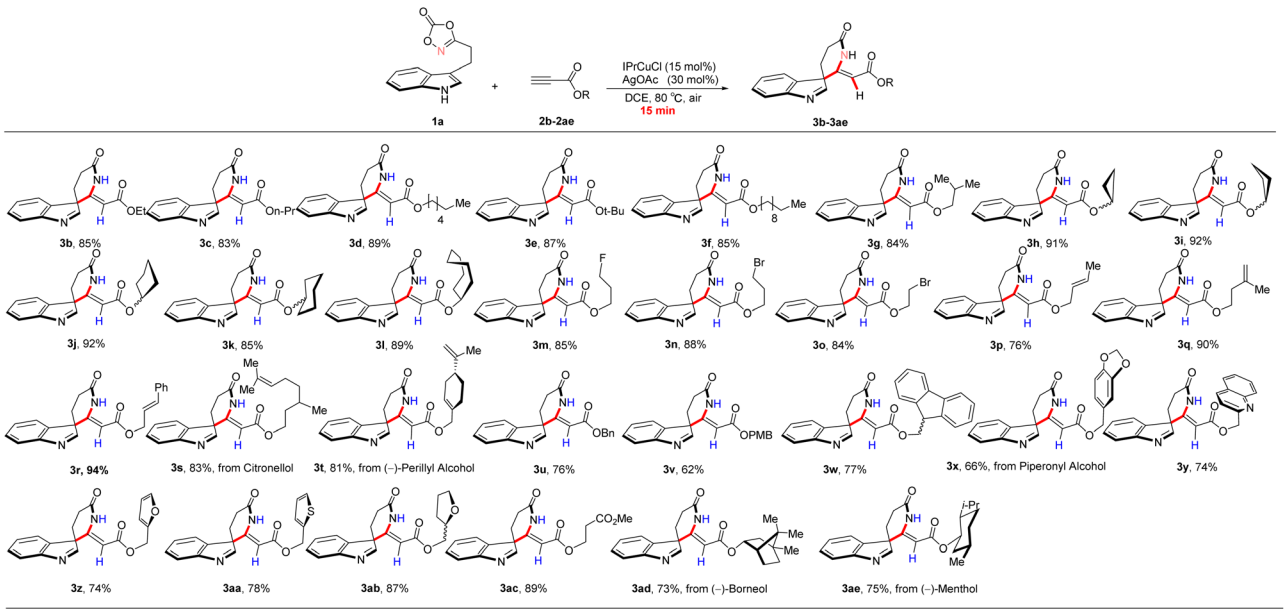

Scheme 2 Substrate scope of various esters [a]Reaction conditions: **1a** (0.20 mmol), **2a** (0.60 mmol), IPrCuCl (15 mol%), AgOAc (30 mol%), 80 °C, 15 min, 0.05 M, under air. [b]Isolated yields. *Z*/*E* > 20 : 1. Abbreviations: DCE = 1,2-dichloroethane; Bn = benzyl; PMB = *p*-methoxybenzyl.

ester derivatives were examined to assess the generality of the transformation. Notably, elongation of the alkyl chain (methyl, ethyl, propyl, *tert*-butyl, *sec*-butyl, hexyl, nonyl) was well tolerated, affording the corresponding products (**3a–3g**) in 83–89% isolated yields with excellent stereoselectivity (*Z*/*E* > 20 : 1). Cycloalkyl substituents, including cyclopropyl, cyclobutyl, cyclopentyl, cyclohexyl, and cycloheptyl groups, were also well tolerated under the optimized conditions, delivering the corresponding products (**3h–3l**) in 75–92% isolated yields. Moreover, a variety of functional groups were compatible with the reaction system. Substrates bearing halogens (Br, F), alkenyl moieties, ether linkages, and ester functionalities provided the desired products in good to excellent yields, for example, compounds **3m–3o** (75–88%), **3q–3t** (81–94%), **3ab** (87%), and **3ac** (89%). These transformations proceeded with high efficiency, excellent regioselectivity, and outstanding *Z*/*E* stereoselectivity, thereby establishing a robust platform for subsequent functional group derivatization. Both unsubstituted aryl and electron-rich aryl substrates exhibited good reactivity under the optimized conditions, affording product **3u–3aa** in 66–78% isolated yields, respectively. To evaluate the influence of chiral induction on the formation of the quaternary carbon center, enantioenriched ester substrates were employed. Under the optimized conditions, products **3ad** and **3ae** were obtained

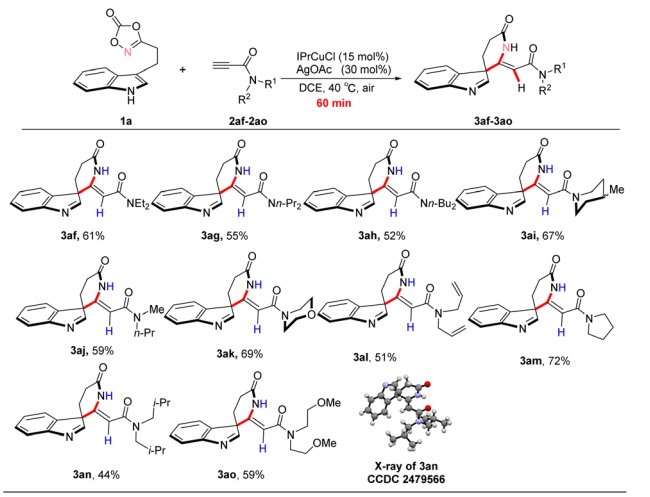

Scheme 3 Substrate scope of various amides [a]Reaction conditions: **1a** (0.20 mmol), **2a** (0.60 mmol), IPrCuCl (15 mol%), AgOAc (30 mol%), 40 °C, 60 min, 0.05 M, under air. [b]Isolated yields. *Z*/*E* > 20 : 1. Abbreviation: DCE = 1,2-dichloroethane.

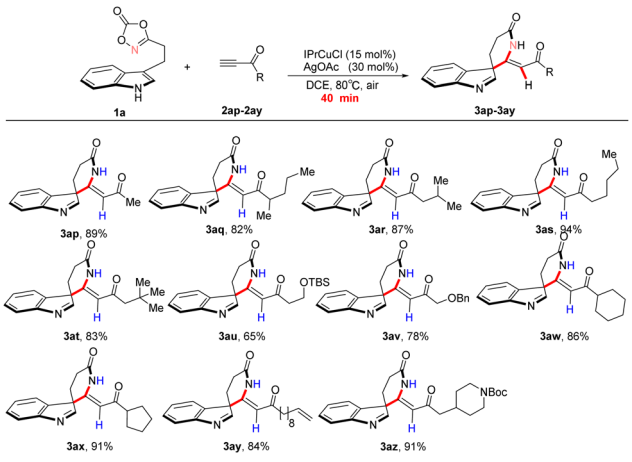

Scheme 4 Substrate scope of various ketones [a]Reaction conditions: **1a** (0.20 mmol), **2a** (0.60 mmol), IPrCuCl (15 mol%), AgOAc (30 mol%), 80 °C, 40 min, 0.05 M, under air. [b]Isolated yields. *Z*/*E* > 20 : 1. Abbreviations: DCE = 1,2-dichloroethane. TBS = *tert*-butyldimethylsilyl, Boc = *t*-butyloxycarbonyl.

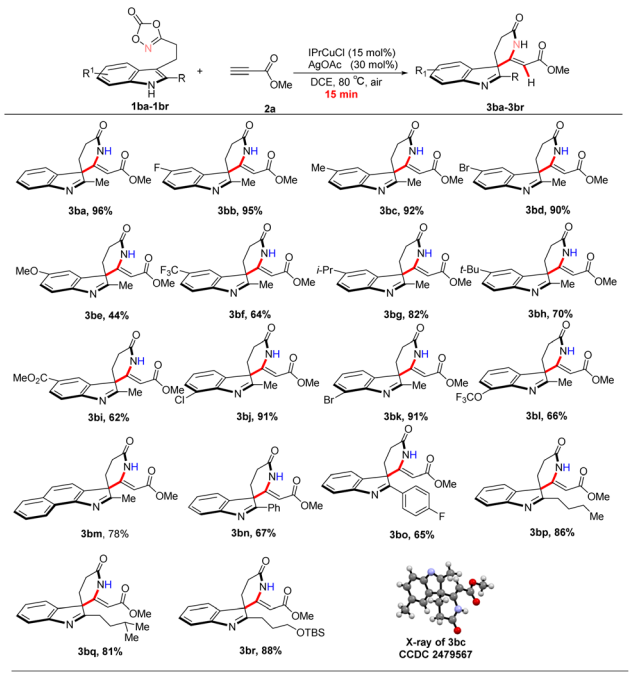

Scheme 5 Substrate scope of various indoles [a] Reaction conditions: **1a** (0.20 mmol), **2a** (0.60 mmol), IPrCuCl (15 mol%), AgOAc (30 mol%), 80 °C, 15 min, 0.05 M, under air. [b]Isolated yields. *Z*/*E* > 20 : 1. Abbreviations: DCE = 1,2-dichloroethane, TBS = *tert*-butyldimethylsilyl.

in 73% and 75% isolated yields, respectively. Notably, NMR analysis revealed no detectable formation of diastereoisomeric mixtures, indicating high stereochemical fidelity during the transformation.

Subsequently, amide derivatives were examined further to expand the substrate scope (Scheme 3). Acyclic amide substrates were poorly compatible under the optimized conditions, affording products **3af–3ah**, **3aj**, **3al**, **3an**, and **3ao** in moderate yields (44–61%). In contrast, cyclic amide substrates were better tolerated, delivering products **3ai**, **3ak**, and **3am** in improved yields of 62–72%. These results suggest that steric and conformational effects associated with the amide moiety significantly influence the reaction efficiency.

Ketone derivatives were subsequently evaluated further to explore the substrate scope (Scheme 4). The reaction demonstrated broad substrate generality and excellent functional group tolerance, affording products **3ap–3at** in 82–94% isolated yields. Notably, the protocol was compatible with various sensitive functional groups, including silyl ethers, benzyl ethers, and alkenes (**3au**, **3av**, **3ay**). In addition, cyclic ketone substrates were well accommodated, delivering products **3aw**, **3ax**, and **3az** in good yields.

The effect of substituents on the indole framework was further examined (Scheme 5). The parent substrate afforded compound **3ba** in 96% isolated yield. Alkyl substituents at the C5 position were well tolerated, providing products **3bb–3bd** and **3bg–3bh** in excellent yields. In contrast, the presence of a strong electron-donating group at C5 significantly reduced the yield to 44% (**3be**), whereas electron-withdrawing substituents provided the corresponding products **3bf** and **3bi** in moderate yields of 62–64%.

At the C7 position, Cl and Br substituents were well tolerated, affording products **3bj–3bk** in 91% isolated yields. In contrast, the introduction of a trifluoromethoxy (CF_3O) group resulted in a 66% yield. Benzoindole was also compatible under the optimized conditions, serving as a precursor to the structurally complex polycyclic product **3bm** in 78% isolated yield. Substitution at the C2 position revealed notable steric effects: bulky aryl substituents led to reduced yields of 65–67% (**3bo**, **3bp**), whereas alkyl groups at C2 were better accommodated, delivering products **3bp–3br** in 81–88% isolated yields.

To gain insight into the reaction mechanism (Scheme 6), a series of control experiments was conducted to systematically assess the roles of the catalyst, additive, and methyl propiolate. The results confirmed that IPrCuCl is essential for catalytic

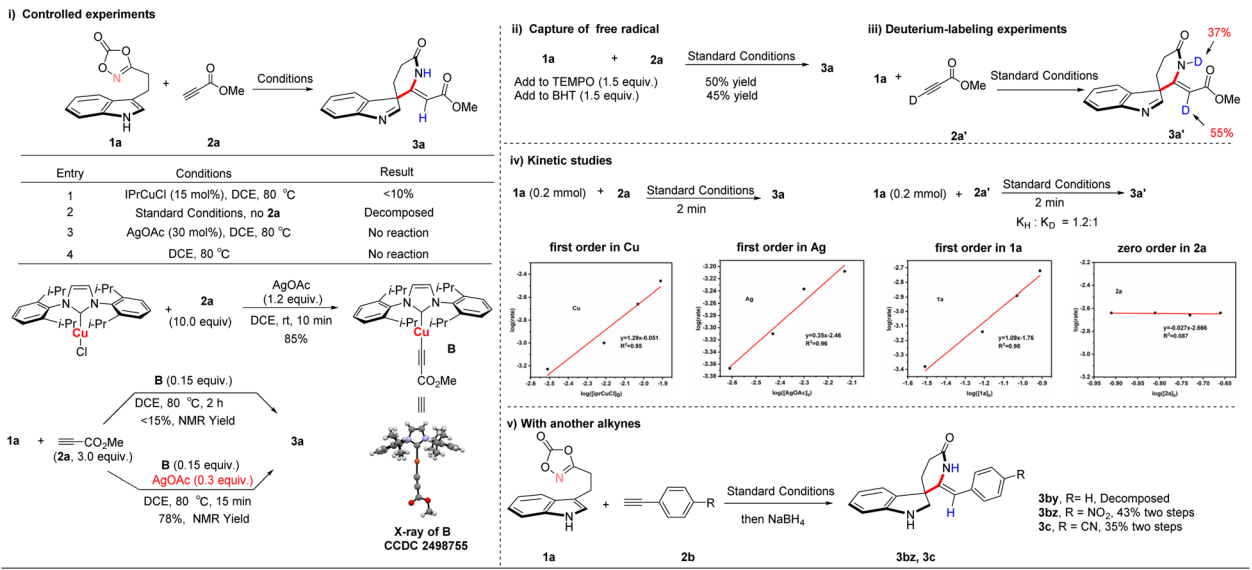

Scheme 6 Mechanistic investigations.

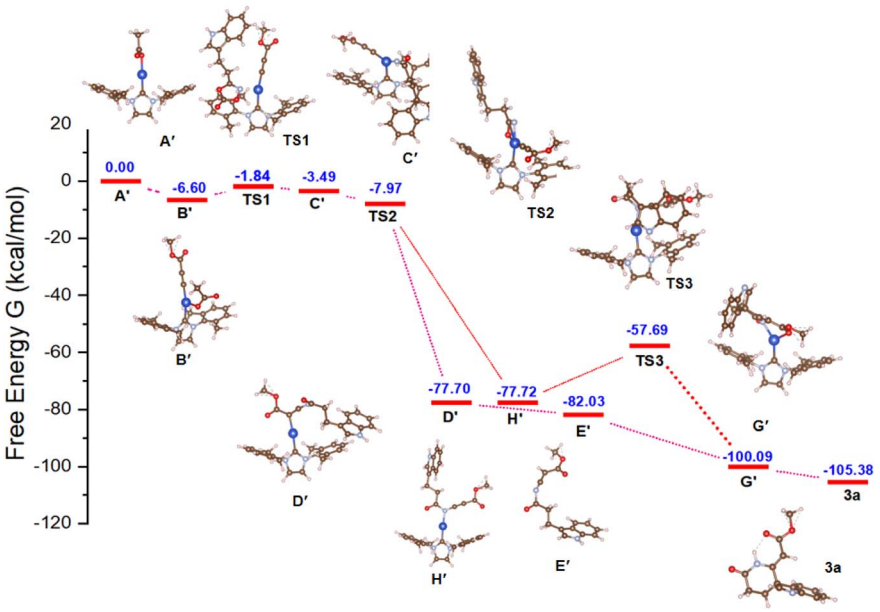

Fig. 1 DFT-computed energy profile for the NHC-Copper-Catalyzed reaction (B3LYP-D3(BJ)).

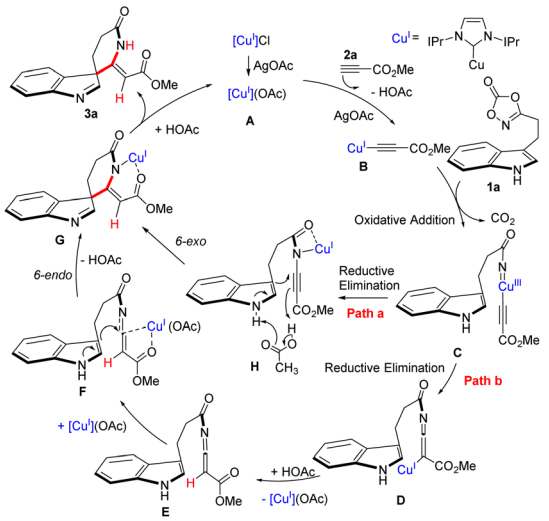

Scheme 7 Proposed reaction mechanism.

activity, while silver acetate functions as a critical additive. To further elucidate the role of silver acetate, complex **B** was successfully isolated and evaluated. This complex exhibited limited catalytic activity, affording the product in less than 15% yield as determined by NMR analysis. Notably, supplementation with additional silver acetate significantly increased the NMR yield to 78%. This result suggests that silver acetate facilitates the formation of complex **B** and that the acetate anion plays a crucial role in promoting hydrogen atom transfer (Scheme 6(i)). Furthermore, radical trapping experiments were conducted using TEMPO and BHT. In both cases, the desired products were still obtained, indicating that the transformation does not proceed *via* a radical-mediated pathway (Scheme 6(ii)). Deuterium labeling experiments provided clear evidence for the migration of the alkynyl hydrogen atom, supporting a 1,1-addition mechanism (Scheme 6(iii)). Kinetic isotope effect (KIE) studies further revealed that copper-alkyne coordination is unlikely to be the rate-determining step. Kinetic analysis established a first-order dependence on the copper catalyst, substrate **1a**, and the silver additive, while exhibiting zero-order dependence on alkyne substrate **2a** (Scheme 6(iv), see SI for detailed kinetic data). These results indicate that metallonitrene formation constitutes the turnover-limiting step in the catalytic cycle. To further substantiate the critical role of copper catalysis in the spirocyclization process, representative terminal alkynes, including phenylacetylene, *p*-nitrophenylacetylene, and *p*-cyanophenylacetylene, were examined (Scheme 6(v)). While the electron-deficient alkynes (*p*-nitro and *p*-cyano) generated the corresponding spirocyclic intermediates, these products were found to be unstable under the reaction conditions. Subsequent reduction with $NaBH_4$ afforded the corresponding stable derivatives (**3bz**, **3c**). NMR analysis confirmed the absence of detectable diastereomeric mixtures. These observations further emphasize the critical role of copper catalysis in enabling the spirocyclization transformation.

Additional mechanistic insights were obtained from density functional theory (DFT) calculations (Fig. 1; see the SI for computational details). To reduce computational cost while preserving steric and electronic features, the 2,6-diisopropylphenyl in IPrCuCl was replaced with 2,6-dimethylphenyl groups to generate the model complex **A′**. The DFT results indicate that the reaction of **A′** with methyl propiolate to form intermediate **B′** is exothermic by 6.60 kcal mol^{-1}. This thermodynamic favorability is consistent with the experimental isolation of intermediate **B** at ambient temperatures. The initial coordination of the dioxazolone nitrogen atom to the copper center and the subsequent bond

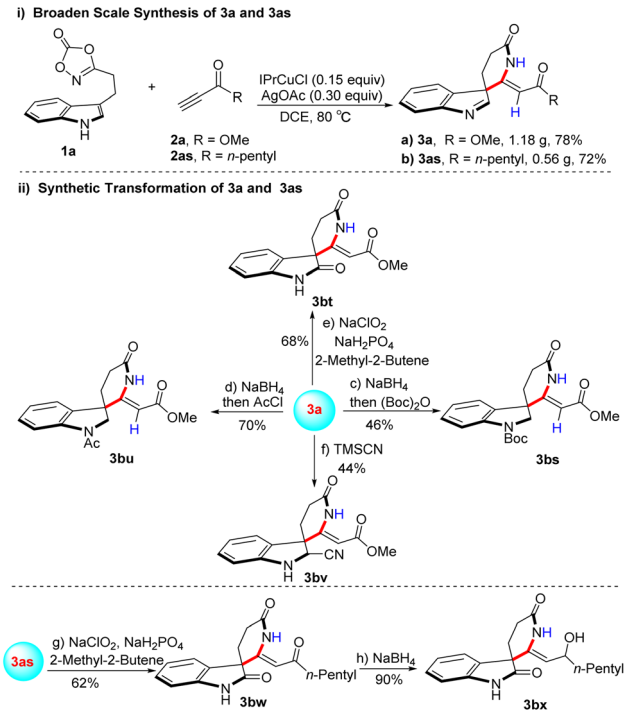

Scheme 8 Gram-scale synthesis and synthetic transformations of **3a** and **3as** [a]Reaction conditions: (a) **1a** (6.60 mmol), **2a** (19.80 mmol, 3.0 equiv.), IPrCuCl (15 mol%), AgOAc (30 mol%), DCE (15 mL), 80 °C, air; (b) **1a** (6.60 mmol), **2as** (19.80 mmol, 3.0 equiv.), IPrCuCl (15 mol%), AgOAc (30 mol%), DCE (15 mL), 60 °C; (c) **3a** (0.20 mmol), $NaBH_4$ (0.24 mmol, 1.2 equiv.), MeOH (10 mL), 0 °C-rt., then $(Boc)_2O$ (2.4 mmol), THF (10 mL), rt.; (d) **3a** (0.20 mmol), $NaBH_4$ (0.24 mmol, 1.2 equiv.), MeOH (10 mL), 0 °C-rt., then Et_3N (0.6 mmol, 3.0 equiv.), ethanoyl chloride (0.30 mmol, 1.5 equiv.), CH_2Cl_2 (10 mL), 0 °C-rt; (e) **3a** (0.20 mmol), 2-methyl-2-butene (2.20 mmol, 11.0 equiv.), $NaClO_2$ (1.14 mmol, 5.7 equiv.), NaH_2PO_4 (1 M in H_2O, 0.34 mmol, 1.7 equiv.), THF (5 mL), 0 °C-rt; (f) **3a** (0.20 mmol), TMSCN (0.60 mmol, 3.0 equiv.), THF/MeOH (6 mL/3 mL), 0 °C-rt. DCE = 1,2-dichloroethane, THF = tetrahydrofuran; (g) **3as** (0.2 mmol), 2-methyl-2-butene (2.20 mmol, 11.0 equiv.), $NaClO_2$ (1.14 mmol, 5.7 equiv.), NaH_2PO_4 (1 M in H_2O, 0.34 mmol, 1.7 equiv.), THF (5 mL), 0 °C-rt; (h) **3bw** (0.20 mmol), $NaBH_4$ (0.24 mmol, 1.2 equiv.), MeOH (10 mL), 0 °C-rt. $(Boc)_2O$ = Di-*tert*-butyl dicarbonate. AcCl = ethanoyl chloride. TMSCN = trimethylsilyl cyanide.

formation proceed through an endothermic transition state (**TS1**). In contrast, extrusion of CO_2 to generate the thermodynamically stable chelated intermediate **C′** is energetically favorable and exothermic. Notably, the calculated energy difference between the **C′** → **D′** and **C′** → **H′** pathways is only 0.01 kcal mol^{-1}, indicating that both pathways are energetically comparable and may competitively operate under the reaction conditions. The formation of intermediate **E′** was calculated to be thermodynamically favorable, consistent with time-resolved *in situ* ^1H NMR monitoring (see SI). In contrast, analysis of the **H–G** transition state indicates that the proton migration step is associated with a relatively high activation barrier, suggesting that hydrogen transfer may be kinetically demanding within the catalytic cycle.

Based on experimental observations and literature reports,[42,51–54] a plausible catalytic mechanism is proposed (Scheme 7). Initially, the Cu^I precatalyst coordinates with AgOAc to generate the active copper complex **A**. Subsequently, complex **A** reacts with methyl propiolate in the presence of AgOAc to afford the alkynyl copper intermediate **B**. Subsequent N–O bond cleavage of the dioxazolone, accompanied by CO_2 extrusion, generates a copper-nitrenoid intermediate, which furnishes complex **C** *via* metal-nitrenoid insertion. From intermediate **C**, the catalytic cycle may proceed through reductive elimination to form either species **D** or **H**. Protonation of complex **D** then affords intermediate **E**, a step associated with hydrogen migration within the spirocyclic framework. To promote the 6-*endo* cyclization, Cu^I likely functions as a Lewis acid, facilitating the conversion of intermediate **E** to **F** (Path a). Alternatively, complex **H** may undergo proton migration to generate **F** (Path **b**). Intermediate **F** subsequently undergoes intramolecular 6-*endo* cyclization to form complex **G.** Finally, proton migration from **G** delivers the spiroindole δ-lactam product **3a**, thereby completing the catalytic cycle.

To further evaluate the practical applicability of this methodology, gram-scale synthesis and subsequent synthetic transformation of **3a** and **3as** were investigated (Scheme 8). Under scaled-up conditions, compounds **3a** and **3as** were successfully converted into the corresponding dioxazolone derivatives in 78% and 72% isolated yields, respectively (Scheme 8(i)). Compound **3a** underwent reduction followed by protection to afford derivative **3bs** in 56% isolated yield[55]. Subsequent acetylation with acetyl chloride (AcCl) proceeded smoothly, delivering compound **3bu** in excellent yield (Scheme 8(ii)).[56] Oxidation of **3a** furnished **3bt** in 68% isolated yield,[57] while nucleophilic addition of trimethylsilyl cyanide (TMSCN) provided **3bv** in 44% isolated yield.[58] Similarly, oxidation of **3as** afforded **3bw** in 62% isolated yield, and subsequent reduction of **3bw** gave **3bx** in 90% isolated yield.

Conclusions

In summary, we have developed a novel, operationally simple, and efficient NHC copper-catalyzed strategy for the synthesis of spiroindole δ-lactams from dioxazolones and alkyne derivatives. The methodology exhibits high atom economy, consistently excellent yields, broad functional group tolerance, and outstanding *Z*-selectivity, thereby providing a valuable platform for the construction of structurally complex spirocyclic lactam frameworks. Mechanistic investigations revealed, for the first time, migration of the terminal alkyne hydrogen atom, leading to a distinctive 1,1-addition pathway that enables subsequent indole dearomatization. This transformation not only expands the mechanistic understanding of dioxazolone-alkyne reactivity but also establishes a novel and conceptually distinct synthetic strategy for the construction of spiroindole δ-lactam frameworks.

Author contributions

Z. R. and T. F. contributed equally to this work. Z. R. and Y. Z. conceived, designed, and wrote the manuscript. All authors discussed the results and commented on the manuscript.

Conflicts of interest

The authors declare no competing interests.

Data availability

CCDC 2479571, 2479566, 2479567 and 2498755 contain the supplementary crystallographic data for this paper.[59a–d]

All other relevant data generated an analysed during this study are included in this article and its supplementary information (SI). Source data are provided with this paper. Supplementary information: experimental, spectroscopic, crystallographic and computational data. See DOI: https://doi.org/10.1039/d5sc09742h.

Acknowledgements

We acknowledge financial support from the National Natural Science Foundation of China (NSFC, No. 22301264). National Science of foundation of Shannxi Province (2023-JC-QN-0135, 2024JC-YBQN-0083), and Research Program of Yan'an University (YAU202407417).

Notes and references

1 E. Chupakhin, O. Babich, A. Prosekov, L. Asyakina and M. Krasavin, *Molecules*, 2019, **24**, 4165.
2 C. V Galliford and K. A. Scheidt, *Angew. Chem., Int. Ed.*, 2007, **46**, 8748–8758.
3 L. Yu, A. Dai, W. Zhang, A. Liao, S. Guo and J. Wu, *J. Agric. Food Chem.*, 2022, **70**, 10693–10707.
4 L. Chen, Q. J. Ding, J. J. Liu, S. Yang and Z. M. Zhang, Preparation of spiroindolinone derivatives as antiproliferative and anticancer agents. 2007, *US pat.*
5 Q. Ding, J. J. Liu and Z. Zhang, Preparation of spiroindolinone derivatives as antitumor agents, WO2007104714A1, 2007.
6 M. J. Kornet and A. P. Thio, *J. Med. Chem.*, 1976, **19**, 892–898.
7 C. J. Barrow and H. H. Sun, *J. Nat. Prod.*, 1994, **57**, 471–476.
8 T. O. Larsen, K. Frydenvang, J. C. Frisvad and C. Christophersen, *J. Nat. Prod.*, 1998, **61**, 1154–1157.
9 R. D. Grigg, J. W. Rigoli, S. D. Pearce and J. M. Schomaker, *Org. Lett.*, 2012, **14**, 280–283.
10 T. R. Roose, D. S. Verdoorn, P. Mampuys, E. Ruijter, B. U. W. Maes and R. V. A. Orru, *Chem. Soc. Rev.*, 2022, **51**, 5842–5877.
11 R. H. Morris, *Chem. Soc. Rev.*, 2024, **53**, 2808–2827.
12 W. Wang, J. Wang, Y. Wang and Z. Xu, *Chin. J. Chem.*, 2025, **43**, 3221–3226.
13 J. Miao, Z.-X. Yu, C.-Y. Shi, X.-Q. Zhu, B. Zhou and L.-W. Ye, *J. Org. Chem.*, 2025, **37**, 13201–13211.
14 S. Xie, S. Tang, M. Hou, W. Xie, M. Guan, T. Bai, L. He and G. Qiu, *Org. Lett.*, 2024, **26**, 11134–11139.
15 E. T. Marris, D. S. Rampon and J. M. Schomaker, *Acc. Chem. Res.*, 2025, **58**, 231–249.
16 X. Lai, J.-B. Liu, Y.-C. Wang and G. Qiu, *Chem. Commun.*, 2021, **57**, 2077–2080.
17 J.-B. Liu, M. Ren, X. Lai and G. Qiu, *Chem. Commun.*, 2021, **57**, 4259–4262.
18 Q. Wang and J. A. May, *Org. Lett.*, 2020, **22**, 3039–3044.
19 K. Hong, S. Zhou, W. Hu and X. Xu, *Org. Chem. Front.*, 2020, **7**, 1327–1333.
20 J. R. Corbin, D. R. Ketelboeter, I. Fernández and J. M. Schomaker, *J. Am. Chem. Soc.*, 2020, **142**, 5568–5573.
21 K. Hong, H. Su, C. Pei, X. Lv, W. Hu, L. Qiu and X. Xu, *Org. Lett.*, 2019, **21**, 3328–3331.
22 R. A. Brawn, K. Zhu and J. S. Panek, *Org. Lett.*, 2014, **16**, 74–77.
23 A. R. Thornton and S. B. Blakey, *J. Am. Chem. Soc.*, 2008, **130**, 5020–5021.
24 A. R. Thornton, V. I. Martin and S. B. Blakey, *J. Am. Chem. Soc.*, 2009, **131**, 2434–2435.
25 A. H. Stoll and S. B. Blakey, *J. Am. Chem. Soc.*, 2010, **132**, 2108–2109.
26 N. Mace, A. R. Thornton and S. B. Blakey, *Angew. Chem., Int. Ed.*, 2013, **52**, 5836–5839.
27 X. Lyu, J. Zhang, D. Kim, S. Seo and S. Chang, *J. Am. Chem. Soc.*, 2021, **143**, 5867–5877.
28 S. Y. Hong, J. Son, D. Kim and S. Chang, *J. Am. Chem. Soc.*, 2018, **140**, 12359–12363.
29 H. Choi, X. Lyu, D. Kim, S. Seo and S. Chang, *J. Am. Chem. Soc.*, 2022, **144**, 10064–10074.
30 S. Gong, S.-H. Wang, Z.-L. Wang and W.-M. He, *Adv. Synth. Catal.*, 2025, **367**, DOI: 10.1002/adsc.70158.
31 K. M. Vliet and B. de Bruin, *ACS Catal.*, 2020, **10**, 4751–4769.
32 J.-J. Tang, N. Yan, Y. Zhang, Y. Wang, M. Bao and X. Yu, *Green Chem.*, 2023, **25**, 7529–7533.
33 Y. Du, X. Yu, J.-J. Tang, Y. Li, J. Fan, F. Li and M. Bao, *J. Org. Chem.*, 2023, **88**, 9783–9790.
34 J.-J. Tang, X. Yu, Y. Wang, Y. Yamamoto and M. Bao, *Angew. Chem., Int. Ed.*, 2021, **60**, 16426–16435.
35 S. Kim, S. L. Song, J. Zhang, D. Kim, S. Hong and S. Chang, *J. Am. Chem. Soc.*, 2023, **145**, 16238–16248.
36 S. Zhou, T. Liu and X. Bao, *J. Catal.*, 2022, **415**, 142–152.
37 H. Wang, H. Jung, F. Song, S. Zhu, Z. Bai, D. Chen, G. He, S. Chang and G. Chen, *Nat. Chem.*, 2021, **13**, 378–385.
38 S.-Y. Zhu, W.-J. He, G.-C. Shen, Z.-Q. Bai, F.-F. Song, G. He, H. Wang and G. Chen, *Angew. Chem., Int. Ed.*, 2024, **63**, e202312465.
39 Z. Bai, S. Zhu, Y. Hu, P. Yang, X. Chu, G. He, H. Wang and G. Chen, *Nat. Commun.*, 2022, **13**, 6445.
40 E. Lee, Y. Hwang, Y. B. Kim, D. Kim and S. Chang, *J. Am. Chem. Soc.*, 2021, **143**, 6363–6369.
41 S. Kim, E. Tufano, M. Barilli, E. Casali, Y. Kim, D. Kim, T. Massimini, G. Zanoni and S. Chang, *J. Am. Chem. Soc.*, 2025, **147**, 38772–38784.
42 K. M. Vliet, L. H. Polak, M. A. Siegle, J. I. Vlugt, C. F. Guerra and B. de Bruin, *J. Am. Chem. Soc.*, 2019, **141**, 15240–15249.
43 T. P. Singh and O. M. Singh, *Mini-Rev. Med. Chem.*, 2018, **18**, 9–25.
44 J. A. Homer and J. Sperry, *J. Nat. Prod.*, 2017, **80**, 2178–2187.
45 A. Mehra, V. Sharma, A. Verma, S. Venugopal, A. Mittal, G. Singh and B. Kaur, *ChemistrySelect*, 2022, **7**, e202202361.

46 M. Pang, H. Chang, Z. Feng and J. Zhang, *Chin. J. Org. Chem.*, 2023, **43**, 1271–1291.
47 L.-M. Yu, H. Chen, W. Fang, R. Cai, Y. Tao, Y. Li and H. Dong, *Org. Biomol. Chem.*, 2024, **22**, 7074–7091.
48 F. Buttard and X. Guinchard, *ACS Catal.*, 2023, **13**, 9442–9475.
49 F.-T. Sheng, J.-Y. Wang, W. Tan, Y.-C. Zhang and F. Shi, *Org. Chem. Front.*, 2020, **7**, 3967–3998.
50 Y. Hwang, Y. Park, Y. B. Kim, D. Kim and S. Chang, *Angew. Chem., Int. Ed.*, 2018, **57**, 13565–13569.
51 T. R. Roose, F. McSorley, B. Groenhuijzen, J. M. Saya, B. U. W. Maes, R. V. A. Orrù and E. Ruijter, *J. Org. Chem.*, 2023, **88**, 17345–17355.
52 A. Makarem, R. Berg, F. Rominger and B. F. Straub, *Angew. Chem., Int. Ed.*, 2015, **54**, 7431–7435.
53 M. K. Armstrong, M. B. Goodstein and G. Lalic, *J. Am. Chem. Soc.*, 2018, **140**, 10233–10241.
54 Z. Ren, T. Feng, T. Gao, B. Han, R. Guo, H. Ma, J.-J. Wang and Y. Zhang, *Org. Lett.*, 2024, **26**(40), 8532–8536.
55 R. Chouhan, H. Bhattacharyya and S. K. Das, *Org. Lett.*, 2024, **26**, 1088–1093.
56 M. Feng, A. J. Fernandes, R. Meyrelles and N. Maulide, *Chem*, 2023, **9**, 1538–1548.
57 X. Zhang, Q. Song, S. Liu, P. Sivaguru, Z. Liu, Y. Yang, Y. Ning, E. A. Anderson, G. D. Ruiter and X. Bi, *Nat. Chem.*, 2025, **17**, 215–225.
58 D.-Y. Zhu, L. Fang, H. Han, Y. Wang and J.-B. Xia, *Org. Lett.*, 2017, **19**, 4259–4262.
59 (*a*) CCDC 2479571: Experimental Crystal Structure Determination, 2026, DOI: 10.5517/ccdc.csd.cc2p765b; (*b*) CCDC 2479566: Experimental Crystal Structure Determination, 2026, DOI: 10.5517/ccdc.csd.cc2p7605; (*c*) CCDC 2479567: Experimental Crystal Structure Determination, 2026, DOI: 10.5517/ccdc.csd.cc2p7616; (*d*) CCDC 2498755: Experimental Crystal Structure Determination, 2026, DOI: 10.5517/ccdc.csd.cc2pw50s.